Reconfigurable OTA Chamber for MIMO Wireless Device Testing

Rashid Mehmood*, Jon W. Wallace†, Michael A. Jensen*
* Electrical and Computer Engineering, Brigham Young University, Provo, UT, USA, r.mehmood@ieee.org, jensen@byu.edu
† Electrical and Computer Engineering, Lafayette College, Easton, PA, USA, wall@ieee.org

***Abstract*—Over-the-air (OTA) testing of wireless devices is accomplished typically either in an expensive multi-antenna OTA chamber that offers high multipath control or a low-cost mode-stirred reverberation chamber that offers limited multipath control. We propose a reconfigurable OTA chamber that offers a high level of multipath control at a low cost. We use finite-difference time-domain simulations and measurements to evaluate the achievable fading distribution and power angular spectrum at the device under test.**

I. Introduction

Modern wireless devices increasingly exploit the complicated nature of electromagnetic propagation, making over-the-air (OTA) testing systems essential for robust device design. In multi-antenna OTA testing [1, 2], the device under test (DUT) is surrounded by multiple antennas – each of which is connected to a channel emulator – in an anechoic chamber. While this technique enables synthesis of a wide range of multipath channels, it can be expensive. Mode-stirred reverberation chambers [3, 4] offer more economical testing, although the ability to control the propagation scenario is limited.

To overcome the challenges associated with these traditional OTA testing procedures, we propose a reverberation chamber whose wall reflections can be reconfigured to control the multipath observed at the DUT. This is accomplished by lining the chamber walls with antennas, some of which are connected to transmitting sources and the remainder of which are terminated in tunable impedances. While we have previously demonstrated the performance of a two-dimensional version of this reconfigurable OTA chamber (ROTAC) using idealized simulations [5] and have shown initial results from a preliminary prototype ROTAC [6], in this work we provide comprehensive finite-difference time-domain (FDTD) simulations and measurements of an improved chamber. The results demonstrate the flexibility in controlling the fading distribution and power angular spectrum (PAS) realized at the DUT and confirm the potential of the ROTAC for providing flexible, low-cost OTA testing.

II. ROTAC Simulations

We model the chamber as a perfect electric conducting (PEC) cube with a side length of 30.5 cm, as shown in Fig. 1. Because the FDTD simulation of a lossless chamber would require very long run times to achieve approximately steady-state operation, we introduce a small loss in the chamber. The conductivity σ required to cause a power loss factor L for a plane wave traveling a distance D is given by

$$\sigma = \frac{\log L}{\eta_0 D}, \tag{1}$$

where η_0 is the free-space intrinsic impedance. We compute σ to achieve $L = 0.2$ dB for $D = 30.5$ cm, which is the propagation distance from wall-to-wall. This means that 1% of the power remains after 100 bounces.

Our simulation frequency and time step are $f = 1/T = 2.524$ GHz and $\Delta t = T/100$, respectively. We run all simulations for a total of 500 periods, representing approximately 200 bounces. The spatial cell size is $\Delta = 3.8$ mm, producing a simulation domain size of $80\times80\times80$ cells.

In the chamber simulations, the top and four side walls are lined with a 3×3 grid of monopoles extending into the chamber as shown in Fig. 1. We also place a uniform circular array (UCA) of 8 monopole antennas with a 6 cm radius centered in the chamber. These monopoles are mounted on a 3.8 mm thick plate of wood with relative permittivity $\epsilon_r = 2$, with the feeding cables to the UCA from the bottom of the

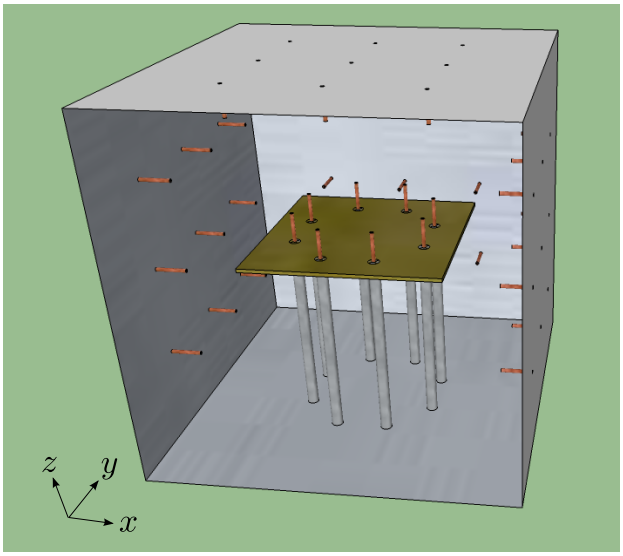

Fig. 1. Model for the FDTD simulations of the ROTAC, where the front panel also lined with a 3×3 grid of monopoles has been removed from the figure to allow visualization of the chamber interior.

ROTAC modeled as PEC cylinders with a radius of 3.8 mm. If $N_{\rm A}$ indicates the total number of antennas, we perform $N_{\rm A}$ FDTD simulations, where for each one a single antenna is excited with unit voltage and internal source impedance of $Z_0 = 50\Omega$ and all other antennas are terminated in Z_0.

We reserve the ports at the center and lower right corner of each chamber wall as feed ports, but excite only one of the ports on each wall at any given time (the other is terminated in an open circuit). We terminate the remaining 7 ports on each wall and all ports on the chamber top with tunable impedances. We compute the S-parameter matrix from the FDTD simulations, and we partition the traveling waves at the ports and the S-parameter matrix as

$$\begin{bmatrix} \mathbf{b}_{\rm U} \\ \mathbf{b}_{\rm E} \\ \mathbf{b}_{\rm T} \end{bmatrix} = \begin{bmatrix} \mathbf{S}_{\rm UU} & \mathbf{S}_{\rm UE} & \mathbf{S}_{\rm UT} \\ \mathbf{S}_{\rm EU} & \mathbf{S}_{\rm EE} & \mathbf{S}_{\rm ET} \\ \mathbf{S}_{\rm TU} & \mathbf{S}_{\rm TE} & \mathbf{S}_{\rm TT} \end{bmatrix} \begin{bmatrix} \mathbf{a}_{\rm U} \\ \mathbf{a}_{\rm E} \\ \mathbf{a}_{\rm T} \end{bmatrix} \qquad (2)$$

where the subscripts U, E, and T indicate the ports corresponding to the UCA, the excitations, and the reconfigurable or open-circuit terminations, respectively. Using that $\mathbf{a}_{\rm T} = \mathbf{\Gamma}_{\rm T}\mathbf{b}_{\rm T}$ where $\mathbf{\Gamma}_{\rm T}$ represents the diagonal matrix of reflection coefficients on the terminated ports and $\mathbf{a}_{\rm U} = \mathbf{0}$ (zero vector) because the UCA ports are terminated in Z_0, we can show that the signals on the UCA ports are given by

$$\mathbf{b}_{\rm U} = \left[\mathbf{S}_{\rm UE} + \mathbf{S}_{\rm UT}\mathbf{\Gamma}_{\rm T}\left(\mathbf{I} - \mathbf{S}_{\rm TT}\mathbf{\Gamma}_{\rm T}\right)^{-1}\mathbf{S}_{\rm TE}\right]\mathbf{a}_{\rm E} \qquad (3)$$

where $\mathbf{I}$ is the identity matrix.

Our model for generating $\mathbf{\Gamma}_{\rm T}$ is based on an experimental reconfigurable impedance element that consists of a tunable varactor diode coupled with additional reactive elements and bias circuitry, as discussed in detail in [7]. This device enables a reflection coefficient phase tuning range of 200° with a maximum power loss of 3 dB over a bias range of 1-5 V. We use this device in our experiments, and we have measured data from this device that allows us to specify the impedance as a function of the bias voltage for our simulations. For all simulations, we realize 5×10^4 random sets of bias voltages, where each voltage is an independent uniformly distributed random variable on $[1, 5]$.

A. Channel Fading

For evaluation of the fading achieved in the chamber, we explore the statistics observed for the signal at a single antenna in the UCA. We excite the center ports on each side wall, with the ℓth port voltage given as $a_{{\rm E},\ell} = e^{j\theta_\ell}$, where θ_ℓ is drawn from a uniform random distribution on $[0, 2\pi)$. If we consider the source to be a unit voltage that is split and shifted in phase as it is fed to the excitation ports, we can consider the scalar value of $b_{\rm U}$ as a channel coefficient that we designate as h. For each random source realization, we compute the channel for all 5×10^4 impedance states. We perform this for 10^4 random source phase realizations and choose the excitation that produces the channel whose magnitude and phase distributions are approximately Rayleigh and uniform, respectively. Fig. 2 shows the result of this computation, revealing that the ROTAC is able to achieve an excellent match to a Rayleigh fading distribution.

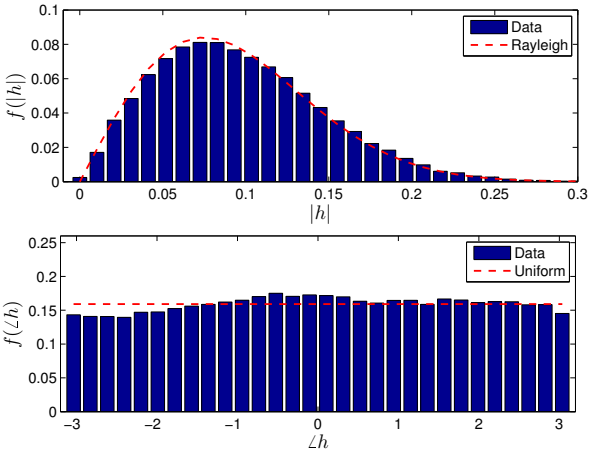

Fig. 2. Simulated magnitude and phase histograms of the channel to one element of the UCA for random loads at the reconfigurable ports.

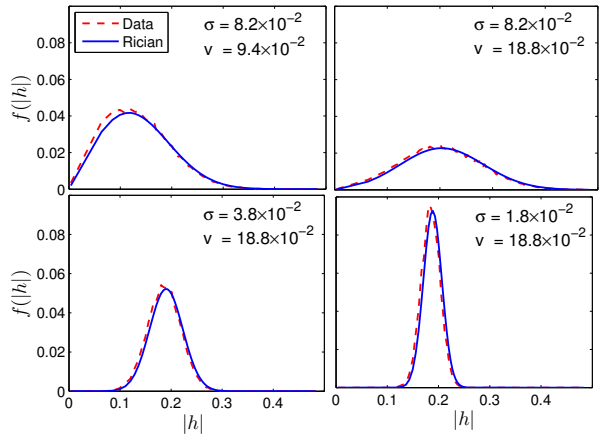

Fig. 3. Simulated pdfs of the magnitude of the channel to one element of the UCA for selected loads at the reconfigurable ports, where in each case the optimization is designed to achieve a Rician distribution for specific values of σ and ν.

To achieve Rician fading, we fix the excitation phases at $\theta_\ell = 0$ and select a subset of the impedance states that achieves the desired channel magnitude distributions. Our target Rician distribution for $\xi = |h|$ is given as

$$f(\xi|\nu,\sigma) = \frac{\xi}{\sigma^2}\exp\left[-\frac{(\xi^2+\nu^2)}{2\sigma^2}\right] I_0\left(\frac{\xi\nu}{\sigma^2}\right) \qquad (4)$$

where $I_0(\cdot)$ is the zeroth-order modified Bessel function of the first kind. Fig. 3 shows the probability density functions (pdfs) of $|h|$ for different target Rician distributions, verifying that the ROTAC is capable of providing a range of fading distributions.

B. Power Angular Spectrum

A major objective of the ROTAC is to synthesize multipath fields with a specified PAS. To accomplish this, we excite the

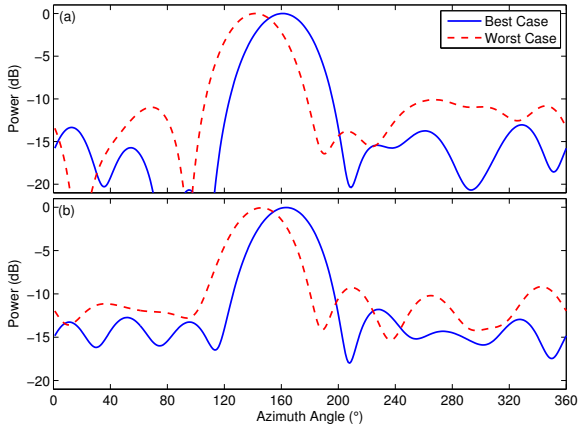

Fig. 4. PAS versus the azimuth arrival angle obtained from the FDTD simulations when the excitation port is at the bottom right of each sidewall. Best and worst PAS (a) for a single reconfigurable impedance realization and (b) averaged over 50 realizations of the reconfigurable impedances.

bottom right port on each side wall, with the excitation on the ℓth port $a_{\mathrm{E},\ell} = c_\ell e^{j\theta_\ell}$ normalized so that $\sum_\ell c_\ell = 1$. We randomly choose 10^3 different complex excitations, and for each excitation we measure the response for all 5×10^4 impedance states. For each realization, we apply a Bartlett beamformer to determine the PAS observed by the UCA, identify the peak of this PAS, and record the sidelobe level (SLL), which is the peak power observed at angles beyond the PAS beamwidth (defined as 40° on either side of the peak). From these combinations, we group all excitations that put a PAS peak at the same azimuth angle and pick the excitation that achieves the lowest SLL for a single termination impedance state as well as the one that achieves the lowest SLL averaged over the best 50 impedance states.

Fig. 4 plots the PAS for the peak angles that achieve the best and worse SLL for a single impedance realization and averaged over 50 impedance realizations. These results demonstrate that 1) the SLL depends somewhat on the peak angle of arrival and 2) while the SLL is higher for the averaged results, the difference is generally small, meaning that a single gain combination can be effective for multiple different reconfigurable impedance states. Most importantly, even the worst case results give a high degree of directivity, demonstrating that it is very feasible to provide a high degree of PAS control in the ROTAC.

III. ROTAC Measurements

Fig. 5 shows photographs of our prototype ROTAC, which is a cube with side length 30.5 cm formed from five aluminum panels. Each of these panels hosts a 3×3 grid of quarter-wave monopole antennas with a 3 inch inter-element spacing, identical to the arrangement used in the simulations. The cube is placed on a ground plane that is perforated with a grid of small holes that allow cable access to a DUT within the chamber, as can be seen in Fig. 5. We measure the fields inside the chamber using a UCA of eight monopole antennas

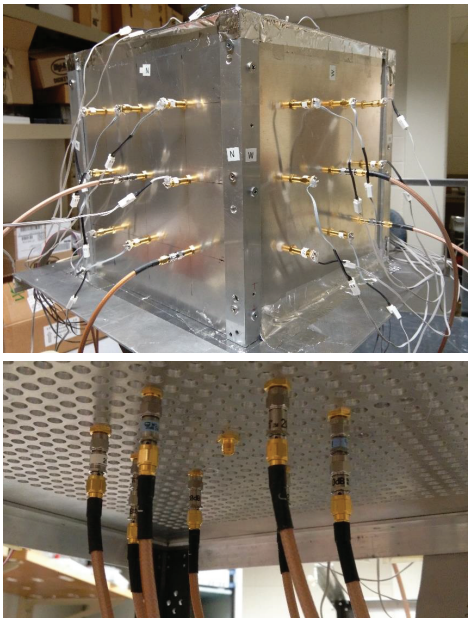

Fig. 5. Photographs of the outside and bottom of the prototype ROTAC.

in the same configuration as used for the FDTD simulations. All measurements are conducted at a frequency of 2.524 GHz.

We again reserve the center and lower right ports on each side panel for excitations and terminate the remaining seven antennas on each side wall and all antennas on the top wall with a tunable impedance. Measurements are performed using an 8×8 multiple-input multiple-output channel sounder [8], where each of four sounder transmit ports is connected to a feed port and the sounder receive ports are connected to the monopole UCA in the middle of the chamber. The sounder channel transfer functions are converted to an S-parameter representation to relate the signals on the UCA antennas to the excitation signals. An FPGA-controlled digital-to-analog converter independently sets the bias voltages applied to the reconfigurable impedances, where we again have 5×10^4 different impedance states.

A. Channel Fading

To explore the fading in the chamber, we again excite the center ports on each side wall and observe the signal on a single antenna of the UCA. We use the same formulation as used above for the FDTD simulations. Figs. 6 and 7 show the results for Rayleigh and Rician fading distributions respectively, with the excellent agreement confirming the conclusions drawn from the simulated results.

B. Power Angular Spectrum

We use the procedure for generating the PAS from the simulated data to the measured responses. Fig. 8 repeats the results of Fig. 4 based on the measured data. The conclusions drawn from the results of the FDTD simulations are confirmed by this experimental validation, and it is encouraging to see

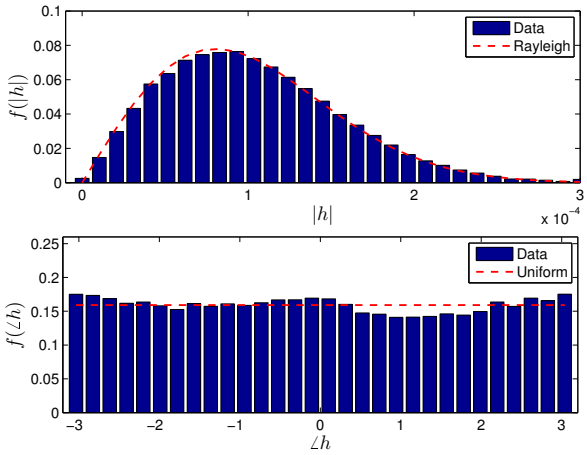

Fig. 6. Measured amplitude and phase histograms of the channel to one element of the UCA for random bias voltages applied to the terminations at the reconfigurable ports.

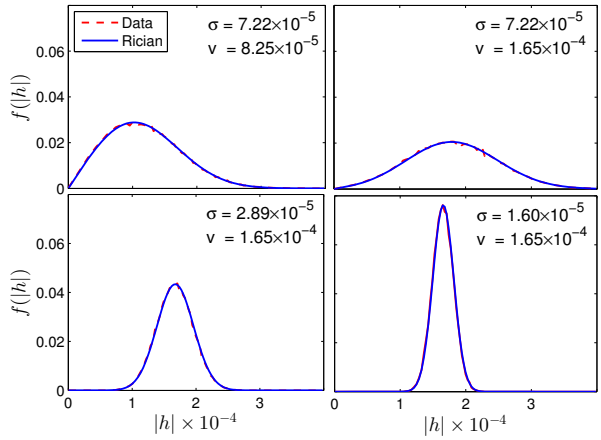

Fig. 7. Measured pdfs of the magnitude of the channel to one element of the UCA for selected loads at the reconfigurable ports, where in each case the optimization is designed to achieve a Rician distribution for specific values of σ and ν.

that the directivity achieved with the measured data essentially matches that obtained from the more ideal simulations.

IV. Conclusion

This paper shows FDTD simulations and measurements of a ROTAC, showing that the technology can generate specified fading statistics and angular field characteristics at the DUT by controlling the reconfigurable impedances along with the excitation applied to a few transmit ports. The results demonstrate that the ROTAC can potentially offer high emulated field control at a relatively low cost.

Acknowledgement

This work was supported in part by the U. S. Army Research Office under Grant # W911NF-12-1-0469.

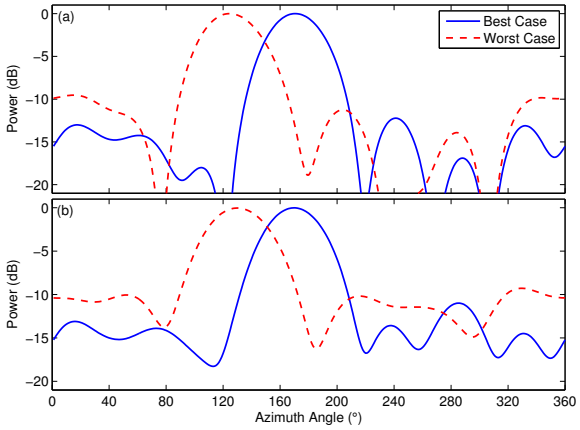

Fig. 8. PAS versus the azimuth arrival angle obtained from measurements when the excitation port is at the bottom right of each sidewall. Best and worst PAS (a) for a single reconfigurable impedance realization and (b) averaged over 50 realizations of the reconfigurable impedances.

References

[1] P. Kyösti, J.-P. Nuutinen, and T. Jamsa, "MIMO OTA test concept with experimental and simulated verification," in *Proc. 4th European Conference Antennas and Propagation (EuCAP)*, Barcelona, Spain, Apr. 12-16, 2010, pp. 1–5.

[2] W. Fan, X. C. B. de Lisbona, F. Sun, J. O. Nielsen, M. B. Knudsen, and G. F. Pedersen, "Emulating spatial characteristics of MIMO channels for OTA testing," *IEEE Transactions on Antennas and Propagation*, vol. 61, no. 8, pp. 4306–4314, 2013.

[3] P.-S. Kildal, C. Orlenius, and J. Carlsson, "OTA testing in multipath of antennas and wireless devices with MIMO and OFDM," *Proceedings of the IEEE*, vol. 100, no. 7, pp. 2145–2157, 2012.

[4] M. A. Garcia-Fernandez, J. D. Sanchez-Heredia, A. M. Martinez-Gonzalez, D. A. Sanchez-Hernandez, and J. F. Valenzuela-Valdes, "Advances in mode-stirred reverberation chambers for wireless communication performance evaluation," *IEEE Communications Magazine*, vol. 49, no. 7, pp. 140–147, 2011.

[5] J. W. Wallace, R. Mehmood, and M. A. Jensen, "Electronically reconfigurable reverberation chambers," in *Proc. 8th European Conference Antennas and Propagation (EuCAP)*, The Hague, The Netherlands, Apr. 6-11, 2014, pp. 3669–3673.

[6] R. Mehmood, J. W. Wallace, and M. A. Jensen, "An experimental reconfigurable OTA chamber," in *Proc. 9th European Conference Antennas and Propagation (EuCAP)*, Lisbon, Portugal, Apr. 12-17, 2015, pp. 1–2.

[7] ——, "Key establishment employing reconfigurable antennas: Impact of antenna complexity," *IEEE Transactions on Wireless Communications*, vol. 13, no. 11, pp. 6300–6310, 2014.

[8] B. T. Maharaj, J. W. Wallace, M. A. Jensen, and L. P. Linde, "A low-cost open-hardware wideband multiple-input–multiple-output (MIMO) wireless channel sounder," *IEEE Transactions on Instrumentation and Measurement*, vol. 57, no. 10, pp. 2283–2289, 2008.